Chemical Engineering Journal 326 (2017) 29–36

Contents lists available at ScienceDirect

Chemical Engineering Journal

journal homepage: www.elsevier.com/locate/cej

Photocatalytic reactors with suspended and immobilized TiO_2: Comparative efficiency evaluation

Agustina Manassero, María Lucila Satuf, Orlando Mario Alfano *

Instituto de Desarrollo Tecnológico para la Industria Química (Universidad Nacional del Litoral and Consejo Nacional de Investigaciones Científicas y Técnicas), predio CONICET "Dr. Alberto Cassano", Ruta Nacional N°168, 3000 Santa Fe, Argentina

HIGHLIGHTS

- Three reactor configurations were evaluated for the degradation of clofibric acid.
- The energy absorbed by the catalyst was computed for each reactor configuration.
- Performances of reactors were evaluated by using photonic and quantum efficiencies.
- The slurry reactor was the most efficient configuration assayed.
- The fixed-bed reactor rendered a satisfactory value of quantum efficiency.

GRAPHICAL ABSTRACT

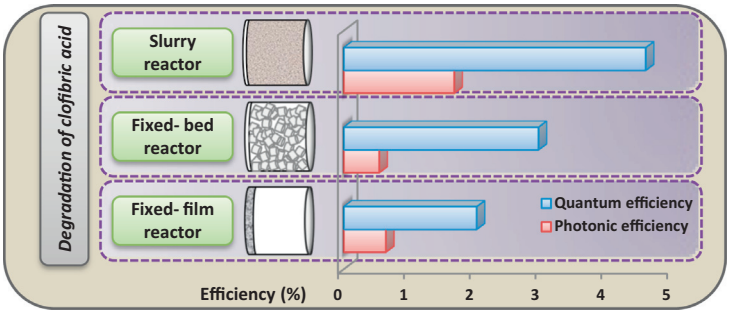

ARTICLE INFO

Article history:
Received 30 December 2016
Received in revised form 12 May 2017
Accepted 13 May 2017
Available online 17 May 2017

Keywords:
Photocatalysis
Efficiency parameters
Wastewater treatment
Reactor design
Slurry reactor
Immobilized catalyst

ABSTRACT

The efficiency of three photocatalytic reactor configurations for the degradation of the micropollutant clofibric acid in water was assessed. The following reaction systems were tested: (i) a slurry reactor with suspended TiO_2 particles; (ii) a fixed-film reactor with TiO_2 immobilized onto the reactor window; and (iii) a fixed-bed reactor filled with TiO_2-coated glass rings. The influence of the catalyst concentration in the suspended system and the number of the catalyst coatings in the immobilized systems were evaluated. The performances of the reactors, under the experimental condition of highest reaction rate for each configuration, were compared with the aid of two parameters: (i) the photonic efficiency (η), which is the ratio of the reaction rate to the rate of incident photons; and (ii) the quantum efficiency (η_{Rxn}), which is the ratio of the reaction rate to the photon absorption rate. The obtained values of η_{Rxn} were 4.59, 2.96 and 2.02% for the slurry reactor, the fixed-bed reactor and the fixed-film reactor, respectively. Although the slurry reactor was the most efficient configuration, the fixed-bed reactor rendered a value of quantum efficiency only one third lower than the suspended system, making this configuration very convenient for photocatalytic reactions. The analysis of the reaction rate, the photon absorption rate and the quantum efficiency are essential to rationally improve the design, configuration and experimental conditions of photocatalytic reactors.

1. Introduction

Photocatalytic slurry reactors with suspended TiO_2 particles are the most common type of reactors employed for research purposes. The main advantage of these reactors is the high specific surface area of catalytic particles in suspension. However, for practical applications, reactors with immobilized TiO_2 are preferred; they allow operation under continuous mode, no separation of catalyst particles is needed, and catalytic supports can be reused for several cycles. The main drawback of immobilized systems is the

* Corresponding author.
E-mail address: alfano@santafe-conicet.gov.ar (O.M. Alfano).

http://dx.doi.org/10.1016/j.cej.2017.05.087
1385-8947/

Nomenclature

A_{cat}	catalytic area (cm^2)
A_{proj}	total sum of the projected area (cm^2)
A_w	reactor window area (cm^2)
C	molar concentration (mol cm^{-3})
CA	clofibric acid
d	diameter of the rings (cm)
e_x	direction cosine (dimensionless)
e^a	local volumetric rate of photon absorption (Einstein cm^{-3} s^{-1})
$e^{a,s}$	local surface rate of photon absorption (Einstein cm^{-2} s^{-1})
FBR	fixed bed reactor
FFR	fixed film reactor
g	asymmetry factor (dimensionless)
L_R	reactor length (cm)
l	length of the rings (cm)
MC	Monte Carlo
MFP	mean free path of photons (cm)
N_{rings}	number of rings in the reactor
n_{ph}	number of photons
$q_{f,in}$	local radiative flux that reaches the TiO_2 film (Einstein s^{-1} cm^{-2})
$q_{f,tr}$	local radiative flux transmitted through the TiO_2 film (Einstein s^{-1} cm^{-2})
$q_{f,rf}$	local radiative flux reflected by the TiO_2 film (Einstein s^{-1} cm^{-2})
q_w	incident radiation flux (Einstein s^{-1} cm^{-2})
SR	slurry reactor
R	reflectance (dimensionless)
R_i	random number
r	reaction rate (mol cm^{-3} s^{-1})
r^s	surface reaction rate (mol cm^{-2} s^{-1})
T	effective transmittance (dimensionless)
t_{TiO_2}	average thickness of the coatings (cm or μm)
t	time (s)
V	volume (cm^3)
x	axial coordinate (cm)
$\boldsymbol{x}$	position vector

Greek letters

α	fraction of energy absorbed by the TiO_2 films (dimensionless)
β	spectral extinction coefficient (cm^{-1})
ξ	length of flight (cm)
φ	normalized fraction of radiation that reaches the coated window (dimensionless)
κ	spectral volumetric absorption coefficient (cm^{-1})
η	photonic efficiency (mol $Einstein^{-1}$)
η_{Rxn}	quantum efficiency (mol $Einstein^{-1}$)
ρ	reflectivity (dimensionless)
θ	spherical coordinate (rad)
σ	volumetric scattering coefficient (cm^{-1})
ω	albedo (dimensionless)

Subscripts

abs	absorbed
CA	clofibric acid
f	relative to a property of the TiO_2 film
fg	relative to a property of the TiO_2 film + glass
g	relative to a property of the bare borosilicate glass plate
λ	dependence on wavelength
R	reactor
T	total
Tk	tank
0	initial condition

Special symbols

$\langle\rangle$	denotes average value over a given space
Δx	length of the cells employed in MC simulations (cm)

low area-to-volume ratio, which can lead to mass transfer limitations and low reaction rates [1]. This disadvantage could be overcome by a proper reactor design, which should tend to maximize catalyst illumination and avoid mass transfer limitations [2,3].

In slurry reactors, the catalyst concentration is one of the most important design parameter because it affects the radiation distribution and, therefore, the photocatalytic activity. Above a certain catalyst dosage, the penetration of the photons in the reactor decreases and thereby, the reaction rate. In the literature, optimal TiO_2 catalyst loading for different systems and reactors has been reported [4–7]. Similarly, in immobilized systems, the thickness of the films is crucial because it directly affects the amount of the light absorbed. This factor has been rigorously analyzed by different research groups [8–10]. Two different illumination configurations are possible in fixed-film reactors: light can be introduced from the support side or from the solution side. In the first configuration, an optimal film thickness renders the maximum reaction rate. Increasing the film thickness beyond the optimal value would be detrimental for the reactor performance. In the second configuration, the reaction rate increases with the film thickness up to a specific value. Further increase in the film thickness does not enhance the reaction rate.

Efficiency parameters are the most adequate tools to evaluate the performance of different reactor configurations [11]. Without them, objective comparison of results from different research studies is not possible. The photonic efficiency (η) is the most frequently reported parameter to compare immobilized and suspended photocatalytic systems. η relates the moles of reactant molecules degraded per mol of incident photons [12,13]. Dijkstra et al. [2] employed this parameter to compare the performance of a tubular reactor with suspended and immobilized TiO_2. The comparison was made under optimal experimental conditions for each configuration, and similar efficiencies were obtained in both systems. Ochuma et al. [14] also employed the photonic efficiency to compare the performance of reactors with suspended titania and titania supported on a reticulated foam monolith. For this comparison, equivalent TiO_2 content in each reactor was employed (e.g. 18.58 g/L in the slurry system and 10 wt.% in the immobilized reactor). Under these particular conditions, higher efficiencies were obtained with supported TiO_2. However, the authors recognize that the opposite situation may take place if TiO_2 concentration in the slurry system is optimized.

In addition, new-defined performance parameters have also been reported in the literature for comparison purposes. Li et al. [15] compared the performance of suspended and immobilized systems based on a ratio between initial reaction rates. More recently, Leblebici et al. [16] compared 12 photocatalytic reactor designs with a new benchmark measure: the photocatalytic space-time yield.

It is important to note that the photonic efficiency considers the amount of photons that arrives at the reactor window or catalytic surface. Taking into account that only the absorbed photons are

employed in photocatalytic reactions, the quantum efficiency parameter is more appropriate to evaluate the performance of photocatalytic systems [17]. The quantum efficiency (η_{Rxn}) relates the moles of pollutant degraded per mol of photons *absorbed* by the catalyst.

In this study, reactors with three different catalyst configurations were compared: a system with suspended TiO_2 particles (slurry reactor, SR) and two immobilized systems: (i) with TiO_2 supported on the illuminated reactor window (fixed film reactor, FFR), and (ii) with TiO_2 immobilized over the surface of glass rings used to fill the reactor (fixed bed reactor, FBR). The same experimental set up was employed in the suspended and immobilized systems. The performances of these configurations were evaluated by means of the photonic efficiency and the quantum efficiency parameters. To the best of our knowledge, this is the first paper to report a rigourous analysis of the radiation absorption and the calculation of the quantum efficiency to objectively compare the performance of a single reactor set up with three different catalyst configurations.

Calculation of the fraction of energy effectively absorbed by the catalyst involves the measurement of the optical properties of the absorbing material and the resolution of radiation models, taking into account the phenomena of absorption and scattering of radiation by TiO_2. In the present work, radiation models in each reactor configuration were solved by the Monte Carlo (MC) method and by the ray tracing technique.

Clofibric acid (CA), the active metabolite of a pharmaceutical employed as blood lipid regulator, was chosen as the model pollutant. Experiments were carried out by varying the catalyst concentration in the slurry reactor and the number of catalyst coatings over the glass supports in the immobilized systems. The reactors were irradiated with UV lamps and TiO_2 P25 was used as catalyst.

2. Experimental

2.1. Reagents and catalytic film preparation

The pharmaceutical clofibric acid (CA, >97%) was obtained from Aldrich. Commercial TiO_2 Aeroxide P25 (Evonik Degussa GmbH, Germany) was employed as photocatalyst.

2.2. Catalyst immobilization

FFR: A circular, flat piece of borosilicate glass of 5 cm diameter was employed as the reactor window, on which the catalyst was immobilized in the FFR. The inner surface of the window, in contact with the liquid, was grounded to improve the adherence of the catalyst to the glass. The external face of the window was covered with tape during the coating procedure.

FBR: Borosilicate glass rings of 0.5 cm (diameter) × 0.5 cm (height) were used as support to immobilize the catalyst in the FBR.

Before the immobilization procedure, the glass pieces (window and rings) were immersed in a washing solution containing 20 g of potassium hydroxide, 250 mL of isopropyl alcohol, and 250 mL of ultrapure water for 24 h. Other remaining traces of organic material were removed by heating at 500 °C for 8 h.

The immobilization of the catalyst over the inner face of the reactor window and over the glass rings (internal and external surfaces) was made by the dip-coating technique. The suspension employed for the coatings was prepared by adding 150 g of powdered TiO_2 in 1000 mL of deionized water with a pH value of 1.5 (adjusted with HNO_3). The glass pieces were dipped into the suspension at room temperature and extracted at a constant withdrawal speed of 3 cm min^{-1} [18]. Afterward, they were dried at 110 °C for 24 h and calcined at 500 °C for 2 h with a heating rate of 5 °C min^{-1}. This procedure was repeated to increase the number of TiO_2 coatings over the supports.

In the case of the rings, the coating procedure involved an additional step. After the withdrawal from the catalyst suspension, the glass pieces were immediately dipped into distilled water to remove the excess of catalyst. This step provided more uniform coatings over the rings.

The adherence of the coatings to the supports was evaluated by recirculating deionized water through both immobilized systems for 6 h. At the end of the tests, no suspended particles of TiO_2 were detected in the water by absorbance measurements, suggesting that the TiO_2 films prepared by the described procedure present good adherence to the glass supports.

2.3. Experimental set up

Experiments were carried out in a batch recirculating system that consists of a glass photocatalytic reactor, a tank with a sampling port, a recirculating pump and a thermostatic bath. Oxygen was supplied through a sparger in the tank. The same experimental set up was employed in the suspended and immobilized systems. The reactor was cylindrical (diameter: 5.00 cm; length: 2.75 cm) with two circular flat windows. It was illuminated through one of the windows, as shown in Fig. 1, by a halogenated mercury lamp (Powerstar HQI-TS 150W/NDL from OSRAM). The lamp, with emission in the UV and visible range, was placed at the focal axis of a parabolic reflector. In order to block the entrance of visible radiation to the reactor, a container with a solution of $CoSO_4$ was interposed between the reactor and the lamp. The wavelengths of the resulting radiation that arrive at the reactor window were comprised between 350 and 410 nm. The incident radiation fluxes at the reactor window in this wavelength range are shown in Table 1. The volume of the empty reactor was 54 mL and the total working volume was 1000 mL. For the SR and FBR, a circular piece of bare borosilicate glass was employed as the reactor window. In the FFR, the bare glass window was replaced by a coated window. A total of 310 coated rings were used to fill the FBR reactor .

Experiments were carried out with different catalyst concentrations and different number of coatings in the suspended and immobilized system, respectively. Experimental conditions are presented in Table 2.

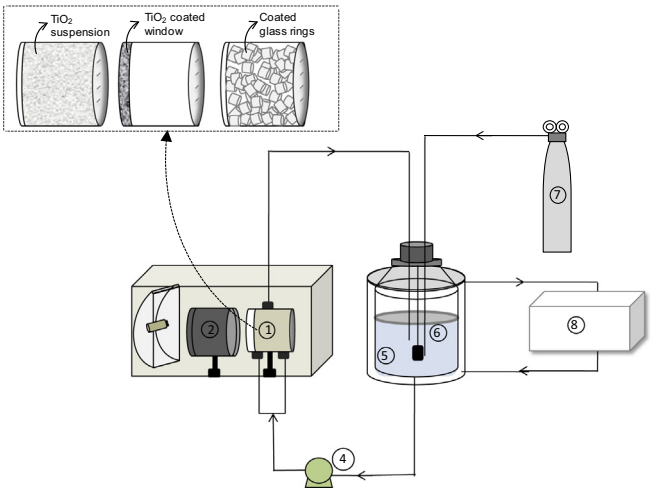

Fig. 1. Schematic representation of the experimental setup: (1) reactor, (2) filter solution, (3) lamp and reflector, (4) pump, (5) tank, (6) thermometer, (7) oxygen and (8) thermostatic bath.

Table 1
Radiation fluxes at the reactor window.

Wavelength (nm)	Radiation flux $\times 10^9$ (Eins s^{-1} cm^{-2})	Radiation flux (mW $cm^{-2)}$
350	0.39	0.13
360	0.89	0.29
370	1.75	0.57
380	2.09	0.66
390	2.82	0.86
400	2.80	0.84
410	3.15	0.92

Table 2
Experimental conditions.

Variable	Value
Initial concentration of CA (mol cm^{-3})	9.30×10^{-8}
pH	Natural (5)
Catalyst concentration in the SR (g L^{-1})	0.1, 0.25, and 0.5
Number of TiO_2 coatings in the FFR and FBR	1, 3, and 5

It should be remarked that additional experiments were carried out to evaluate the effect of calcination on the performance and characteristics of powder TiO_2. Degradation of CA with 0.5 g L^{-1} of calcined and uncalcined TiO_2 P25 for 6 h rendered similar results with a difference in the initial reaction rate of less than 2%; i.e. calcination at 500 °C did not affect the activity of the catalyst in the degradation of CA. Additionally, similar percentages of anatase and rutile phases, crystallinity and crystallite sizes were obtained with calcined and uncalcined samples. Therefore, it can be assured that the calcination procedure carried out in our experiments did not alter the main characteristics of the catalyst, making valid the comparison between suspended and immobilized systems.

2.4. Experimental procedure

Suspended system: The reacting suspension was prepared by adding 20 mg of CA and a defined amount of TiO_2 to a 1000-mL volumetric flask and diluting to volume with ultrapure water. This suspension was sonicated for 30 min and then placed in the tank. At that time, the pump was switched on and the suspension was recirculated in the system for 1 h to reach the adsorption equilibrium of CA onto TiO_2. During this period, the solution was saturated with pure oxygen by intense bubbling in the tank, and the lamp was turned on to stabilize the radiation emission. By means of a shutter, situated between the reactor and the lamp, the reactor was kept in darkness. Then, the first sample was taken and the shutter removed to start the reaction.

Immobilized systems: The reacting solution was prepared by dissolving 20 mg of CA with ultrapure water in a 1000-mL volumetric flask and diluting to volume with the same water. Then, the solution of CA was added to the tank. The following steps were the same as those described for the SR.

2.5. Analysis

CA concentration was measured using HPLC with UV detector (Waters chromatograph provided with a RP C-18 column X-Terra®). The mobile phase was a mixture of acidified water (with 0.1% *v/v* phosphoric acid) and acetonitrile (50:50), pumped at a flow rate of 1.0 mL min^{-1}. The injection volume was 20 μL and the UV detector was set at 227 nm [19]. The samples taken from the suspended system were first centrifuged and then filtered through a 0.02 μm (Anatop 25) to remove TiO_2 particles before analysis.

In the immobilized systems, the mass of TiO_2 per cm^2 of support was quantified by a spectrophotometric technique adapted from Jackson et al. [20]. This technique involves the acidic digestion of the catalyst fixed on the glass support followed by the addition of H_2O_2 to form a colored complex and a photometric detection at 410 nm. A detailed description of the procedure can be found in Zacarías et al. [21].

The thicknesses of the films over the supports were calculated from SEM images acquired by a scanning electron microscope (JEOL, JSM-35C) equipped with an acquisition system of digital images (SemAfore).

3. Theoretical

3.1. Efficiency parameters

The photonic efficiency relates the photocatalytic reaction rate with the rate of incident radiation, according to:

$$\eta = \frac{observed\ reaction\ rate}{rate\ of\ incident\ radiation} \tag{1}$$

As photocatalytic reaction rates are usually reactant concentration dependant (with the exception of zero order reactions), the initial rate is frequently employed in calculations [22].

For the suspended system, η can be expressed as

$$\eta^{susp} = \frac{\langle r_{CA}(\boldsymbol{x}, t_0)\rangle_{V_R} V_R}{\langle q_w(\boldsymbol{x})\rangle_{A_w} A_w} \tag{2}$$

where $\langle r_{CA}(\boldsymbol{x}, t_0)_{V_R}\rangle$ is the initial reaction rate averaged over the reactor volume V_R, and $\langle q_w(\boldsymbol{x})_{A_w}\rangle$ represents the incident radiation flux averaged over the reactor window area, A_w (19.6 cm^2). Similarly, for the immobilized systems, the photonic efficiency can be calculated as

$$\eta^{immob} = \frac{\langle r^s_{CA}(\boldsymbol{x}, t_0)\rangle_{A_{cat}} A_{cat}}{\langle q_w(\boldsymbol{x})\rangle_{A_w} A_w} \tag{3}$$

where $\langle r^s_{CA}(\boldsymbol{x}, t_0)\rangle_{A_{cat}}$ is the initial surface reaction rate averaged over the catalytic area A_{cat}. A_{cat} represents the superficial area of the support that is coated with the catalyst (the porosity of the film or the roughness of the coating are not considered in the calculation). The value of A_{cat} is 19.6 cm^2 in the FFR (area of the circular window) and 467.7 cm^2 in the FBR (sum of the internal and external surfaces of the rings).

The incident radiation flux $\langle q_w(\boldsymbol{x})\rangle_{A_w}$, measured by ferrioxalate actinometry, was 1.39×10^{-8} Einstein/(s cm^2) in all experiments.

On the other hand, the quantum efficiency parameter relates the photocatalytic reaction rate with the radiation absorption rate:

$$\eta_{Rxn} = \frac{observed\ reaction\ rate}{rate\ of\ photon\ absorption} \tag{4}$$

In slurry reactors, where radiation absorption occurs in the whole reactor volume, η_{Rxn} can be expressed as

$$\eta^{Susp}_{Rxn} = \frac{\langle r(\boldsymbol{x}, t_0)\rangle_{V_R}}{\langle e^a(\boldsymbol{x})\rangle_{V_R}} \tag{5}$$

where $\langle e^a(\boldsymbol{x}, t_0)\rangle_{V_R}$ represents the local volumetric rate of photon absorption averaged over the reactor volume V_R.

In reactors with the catalyst immobilized over a surface, η_{Rxn} takes the following form:

$$\eta^{Immob}_{Rxn} = \frac{\langle r^s_{CA}(\boldsymbol{x}, t_0)\rangle_{A_{cat}}}{\langle e^{a,s}(\boldsymbol{x})\rangle_{A_{cat}}} \tag{6}$$

In this case, $\langle e^{a,S}(\boldsymbol{x})\rangle_{A_{cat}}$ represents the local surface rate of photon absorption, averaged over A_{cat}.

In the present study, the initial reaction rate of CA was calculated from experiments, whereas the photon absorption rate was obtained by solving (i) a radiation model in the SR and FBR with the Monte Carlo method or (ii) a radiation balance in terms of local net radiation fluxes in the FFR.

3.2. Reaction rate

To compute the reaction rate, i.e. numerator of Eqs. (2), (3), (5) and (6), the mass balance of CA in each system was considered, making the following assumptions: (i) there is a differential conversion per pass in the reactor, (ii) the system is perfectly stirred, (iii) the chemical reaction occurs only at the solid–liquid interface [23,24], (iv) direct photolysis is neglected, and (v) there are no mass transport limitations. The most likely to be subjected to mass transfer limitations was the fixed-film wall reactor. However, careful analysis and experiments rendered that external and internal mass transfer resistances were negligible [25]. As a result, the mass balance for CA in the system takes the following form:

Suspended catalyst:

$$\left.\frac{dC_{CA}}{dt}\right|_{Tk} = -\frac{V_R}{V_T}\langle r_{CA}(\boldsymbol{x},t)\rangle_{V_R} \tag{7}$$

Immobilized catalyst:

$$\left.\frac{dC_{CA}}{dt}\right|_{Tk} = -\frac{A_{cat}}{V_T}\langle r^s_{CA}(\boldsymbol{x},t)\rangle_{A_{cat}} \tag{8}$$

where C_{CA} is the molar concentration of CA, t denotes reaction time, and V_T is the total system volume.

From Eqs. (7) and (8), the expression for calculating the initial reaction rate in each systems can be derived:

$$\langle r_{CA}(\boldsymbol{x},t_0)\rangle_{V_R} = -\frac{V_T}{V_R}\lim_{t\to 0}\left(\frac{C_{CA}(t)-C_{CA}(t_0)}{t-t_0}\right)_{Tk} \tag{9}$$

$$\langle r^s_{CA}(\boldsymbol{x},t)\rangle_{A_{cat}} = -\frac{V_T}{A_{cat}}\lim_{t\to 0}\left(\frac{C_{CA}(t)-C_{CA}(t_0)}{t-t_0}\right)_{Tk} \tag{10}$$

The term $\lim_{t\to 0}\left(\frac{C_{CA}(t)-C_{CA}(t_0)}{t-t_0}\right)_{Tk}$ was obtained from experimental information by adjusting the data of CA concentration vs. reaction time by an exponential equation and evaluating its derivative at t_0.

3.3. Radiation absorption

3.3.1. Calculation of the photon absorption rate in the SR and FBR

Monte Carlo simulations were carried out to calculate the fraction of radiation absorbed by the catalyst in the SR and the FBR. In these simulations, a great number of photons are traced inside the reactor until they are absorbed or scattered out, and the location of the absorbed photons is recorded. Then, based on these results, it is possible to calculate the spatial distribution of the rate of photon absorption inside the reactor. The direction, length of the trajectory, and fate of the photons are determined by random numbers (R_i) between 0 and 1.

A 1-D radiation model was applied in the calculations. This simplification is possible due to the configuration and dimensions of the reactors: the incoming radiation at the reactor window is diffuse, and the radiation extinction by the catalyst occurs mainly along the longitudinal axis of the cylindrical reactor. Thus, the photon trajectories can be described with one spatial variable (x) and one angular variable (θ). Fig. 2 shows a schematic representation of the coordinate system employed in the model.

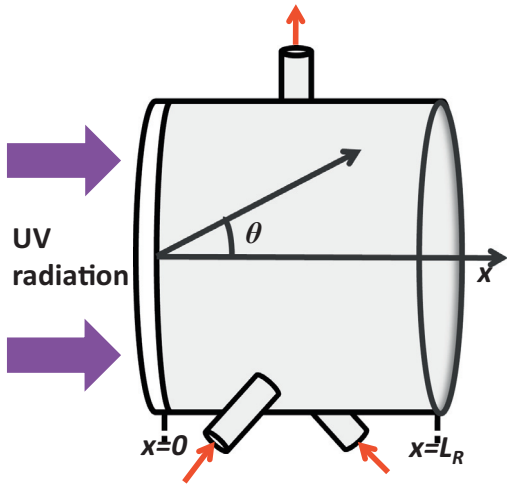

Fig. 2. Schematic representation of the coordinate system.

The emission range of the lamp was discretized into 8 wavelengths and the reactor length L_R was divided into small cells of length Δx to store the position of the absorbed photons. The flowchart of the algorithm employed to calculate the photon absorption rate in both systems is shown in Fig. 3. The main events that were taken into account in the photon tracking are described below:

Photon direction (θ) at the reactor window: Radiation at the inner side of the reactor window is diffuse. Thus, the direction of a photon bundle, determined by the angle θ, has the same probability in all directions [26]:

$$\theta = a\sin(2R_1 - 1) \tag{11}$$

Length of the photon flight (ξ): The distance that a photon can travel in the reacting medium without interactions is determined by Eq. (12) in the SR [27] and by Eq. (13) in the FBR [28].

$$\xi = -\frac{1}{\beta_\lambda}\ln(1-R_2) \tag{12}$$

$$\xi = -MFP\ln(R_2) \tag{13}$$

where β_λ is the spectral extinction coefficient of the catalyst suspension at wavelength λ, and MFP is the mean free path of photons inside the FBR. The MFP was estimated as $MFP = V_R/A_{proj}$. A_{proj} represents the total sum of the projected area of the rings ($A_{proj} = N_{rings}ld$, where N_{rings} is the number of rings in the reactor, and l and d are the length and diameter of an individual ring). The new position (x_{new}) of the photon bundle after traveling the distance ξ in the direction θ is calculated taking into account the previous position of the photon inside the reactor (x_{old}) and the direction cosine (e_x) as follows:

$$x_{new} = x_{old} + e_x\xi \tag{14}$$

Fate of the photon: The spectral albedo is defined as the ratio $\omega_\lambda = \sigma_\lambda/\beta_\lambda$, where σ_λ is the spectral scattering coefficient of the catalyst suspension. In the SR, ω_λ is employed to evaluate whether a photon is absorbed or scattered when it strikes a catalyst particle [26]. Thus, if

$$1 - \omega_\lambda \geqslant R_3 \tag{15}$$

the photon is absorbed. Otherwise, the photon is scattered and the new direction is determined by the Henyey and Greenstein phase function [29]. The cosine of the angle that determines the new direction of the photon is given by [30,31]:

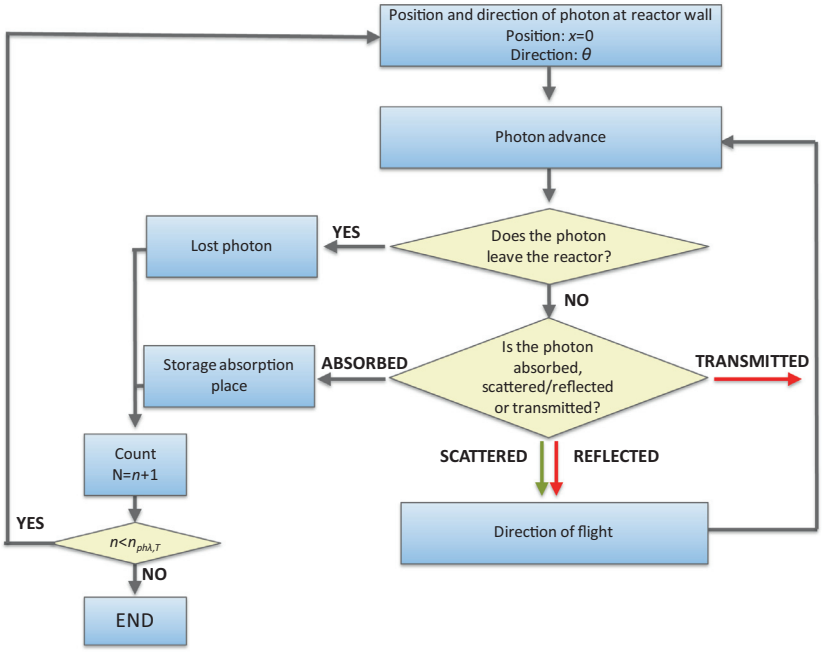

Fig. 3. Flowchart of MC method in the SR and in the FBR. Red arrows: FBR; Green arrows: SR; Grey arrows: SR and FBR. (For interpretation of the references to color in this figure legend, the reader is referred to the web version of this article.)

$$cos\theta = \frac{1}{2g_\lambda}\left[1 + g_\lambda^2 - \left(\frac{1 - g_\lambda^2}{1 + g_\lambda(2R_4 - 1)}\right)^2\right] \tag{16}$$

where g_λ is the asymmetry factor.

On the other hand, in the FBR, the reflectivity (ρ_λ) of the ring wall is employed to evaluate the reflection of photons. If ρ_λ is higher than a new random number (R_3), the photons are reflected. Otherwise, the photons can be absorbed or transmitted. By using the spectral absorption coefficient of the TiO_2 film (κ_λ) and the average thickness of the coatings (t_{TiO_2}), the effective transmittance (T) is calculated according to Eq. (17) [32].

$$T_{TiO_2\ coating} = \exp(-\kappa_\lambda t_{TiO_2}) \tag{17}$$

If T is higher than a new random number R_4, the photons are transmitted; otherwise, the photons are absorbed.

In both systems, when the photons are absorbed, they are stored in the corresponding spatial cell and the trajectory ends. Conversely, if the photons are scattered, reflected or transmitted, the length of the new trajectory is estimated with Eq. (12) in the SR or with Eq. (13) in the FBR, and the sequence continues until the photons are either absorbed or lost outside the reactor.

The local rate of photon absorption at each cell of length Δx is calculated taking into account the number of photons of wavelength λ absorbed in the cell $(n_{ph\lambda,abs})$ and the total number of photons considered in the simulation $(n_{ph,T})$ according to the following equations:

For the SR:

$$e^a(x) = \sum_{\lambda=350\ nm}^{\lambda=410\ nm} \frac{q_{w\lambda} n_{ph\lambda,abs}(x)}{n_{ph,T}\Delta x} \tag{18}$$

For the FBR:

$$e^{a,S}(x) = \sum_{\lambda=350\ nm}^{\lambda=410\ nm} \frac{q_{w\lambda} n_{ph\lambda,abs}(x) V_R}{n_{ph,T}\Delta x A_{cat}} \tag{19}$$

As an example, Fig. 4 shows the profiles of the relative rate of photon absorption in the SR (for 0.5 g L^{-1}) and in the FBR (for 5 TiO_2 coatings). The relative rate of photon absorption is defined as $e^a(x)/e^a(x=0)$ for the SR and $e^{a,s}(x)/e^{a,s}(x=0)$ for the FBR.

In the SR, more than 80% of the total absorbed radiation occurs in the first 0.5 cm of the reactor, leaving a great volume of the reacting solution in the darkness. In contrast, a smoother radiation profile is obtained in the FBR, with a better distribution in the whole reaction space.

Finally, the average value of the photon absorption rate in the reactors is computed as

$$\langle e^a(x)\rangle_{V_R} = \frac{1}{L_R}\int_{x=0}^{x=L_R} e^a(x)dx \tag{20}$$

$$\langle e^{a,S}(x)\rangle_{A_{cat}} = \frac{1}{L_R}\int_{x=0}^{x=L_R} e^{a,S}(x)dx \tag{21}$$

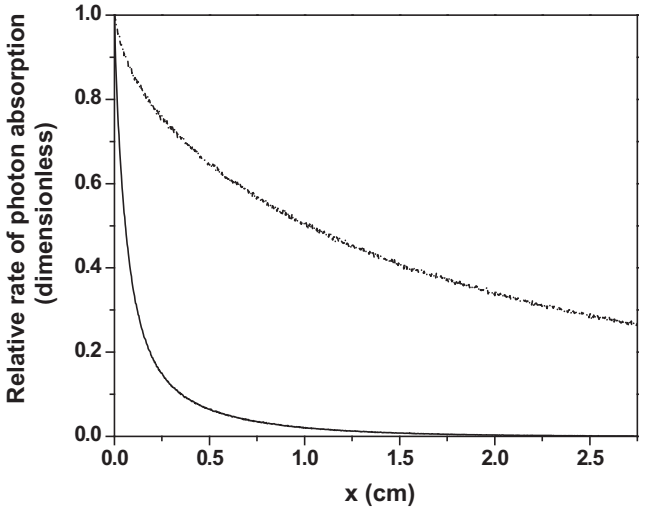

Fig. 4. Profiles of the relative rate of photon absorption in the SR with 0.5 g L^{-1} of TiO_2 (solid line) and in the FBR with 5 catalyst coatings (broken line).

3.3.2. Calculation of the photon absorption rate in the FFR

In order to calculate the $e^{a,s}$ in the FFR, a radiation balance in terms of the local net radiation fluxes in the TiO_2 films is postulated as:

$$\langle e^{a,s}_{f,\lambda}\rangle_{A_{cat}} = \langle q_{f\lambda,in}\rangle_{A_{cat}} - \langle q_{f\lambda,tr}\rangle_{A_{cat}} - \langle q_{f\lambda,rf}\rangle_{A_{cat}} \quad (22)$$

where $q_{f\lambda,in}$ is the local radiative flux that reaches the TiO_2 film, $q_{f\lambda,tr}$ the local radiative flux transmitted through film, and $q_{f\lambda,rf}$ the local radiative flux reflected by the TiO_2 coating. Since the coated window is uniformly irradiated, averaged values of the radiation fluxes over the catalytic area can be employed in calculations. Then, $\langle e^{a,s}_{f,\lambda}\rangle_{A_{cat}}$ can be expressed as a function of the incident radiation flux:

$$\langle e^{a,s}_{f,\lambda}\rangle_{A_{cat}} = \langle q_{f\lambda,in}\rangle_{A_{cat}}\alpha_{f,\lambda} \quad (23)$$

where $\alpha_{f,\lambda}$ is the fraction of radiation absorbed by the film at wavelength λ.

For polychromatic radiation, Eq. (23) can be expressed as:

$$\langle e^{a,s}_{f}\rangle_{A_{cat}} = \langle q_{f,in}\rangle_{A_{cat}}\sum_{\lambda}\alpha_{f,\lambda}\varphi_{\lambda} \quad (24)$$

where φ_{λ} is the normalized fraction of radiation that reaches the coated plate at wavelength λ, and $\sum_{\lambda}$ is the summation over the useful wavelength range. The spectral emission of the lamp, the cut-off effect of the $CoSO_4$ filter and the modification of the lamp spectrum produced by the absorption of the borosilicate glass window were taken into account to obtain φ_{λ}. It should be noted that $\langle q_{f,in}\rangle_{A_{cat}} \equiv \langle q_w(\boldsymbol{x})\rangle_{A_w}$.

The fraction of radiation absorbed by the catalytic film can be calculated as:

$$\alpha_{f,\lambda} = 1 - T_{f,\lambda} - R_{f,\lambda} \quad (25)$$

where $T_{f,\lambda}$ and $R_{f,\lambda}$ represent the fraction of radiation transmitted and reflected by the TiO_2 film at wavelength λ, respectively.

By applying the Net-Radiation method [29] to a coated plate, the values of $T_{f,\lambda}$ and $R_{f,\lambda}$ can be computed as:

$$R_{f,\lambda} = \frac{R_{fg,\lambda}T^2_{g,\lambda} - T^2_{fg,\lambda}R_{g,\lambda}}{T^2_{g,\lambda} - T^2_{fg,\lambda}R^2_{g}} \quad (26)$$

$$T_{f,\lambda} = \frac{T_{fg,\lambda}}{T_{g,\lambda}}(1 - R_{f,\lambda}R_{g,\lambda}) \quad (27)$$

where the subscripts *f*, *g* and *fg* represent the TiO_2 film, the bare glass plate and the coated glass plate, respectively. $R_{fg,\lambda}$, $R_{g,\lambda}$, $T_{fg,\lambda}$ and $T_{g,\lambda}$ were obtained experimentally from diffuse reflectance and transmittance of the coated and bare plates. A detailed description of this methodology can be found in Zacarías et al. [21].

4. Results and discussion

Control experiments were carried out to evaluate direct photolysis of CA and dark reactions in each reactor. No detectable changes occurred in the CA concentration after 5 h of irradiation without catalyst. Additionally, CA was not degraded in the presence of catalyst without illumination, indicating that dark reactions did not take place in the reactors.

Tables 3 and 4 present the values of the apparent kinetic constant *k* obtained from the exponential fitting of the curves of CA concentration vs reaction time $C_{CA}(t) = C_{CA}(t_0)\exp(-kt)$, under different experimental conditions, for the three reactor configurations. The mass of TiO_2 in the reactors is also reported in the tables. Additionally, Table 4 includes the film thickness of the coatings in the immobilized reactors.

Table 3
Apparent kinetic constants and mass of TiO_2 in the SR for different catalyst concentrations.

Catalyst concentration (g L^{-1})	$k \times 10^3$ (min^{-1})	Mass of TiO_2 (mg)
0.1	1.92	5.4
0.25	2.63	13.5
0.5	3.26	27.0

Table 4
Apparent kinetic constants, mass of TiO_2 and film thickness for the different number of catalyst coatings in FFR and FBR.

Number of TiO_2 coatings	FFR			FBR		
	$k \times 10^3$ (min^{-1})	Mass of TiO_2 (mg)	Film thickness (μm)	$k \times 10^3$ (min^{-1})	Mass of TiO_2 (mg)	Film thickness (μm)
1	1.05	3.5	0.65	0.60	7.9	0.11
3	1.23	12.5	1.70	0.87	20.1	0.27
5	1.28	21.2	2.70	1.12	36.5	0.44

Table 5
Efficiency evaluation among SR, FFR and FBR.

Reactor	Condition	Reaction rate × 10^9 (mol s^{-1})	Photon absorption rate × 10^8 (Einstein s^{-1})	η (%)	η_{Rxn} (%)
SR	0.5 g L^{-1}	5.0	10.9	1.68	4.59
FFR	5 coatings	1.9	9.4	0.64	2.02
FBR	5 coatings	1.6	5.4	0.54	2.96

For fair comparison among the three configurations, the condition of maximum reaction rate in each reactor was selected. Maximum reaction rate was reached with 0.5 g L^{-1} of TiO_2 in the SR, and with 5 catalyst coatings in both immobilized systems. The corresponding values of the reaction rate, calculated as $\langle r_{CA}(\boldsymbol{x}, t_0)\rangle_{V_R}V_R$ and $\langle r^s_{CA}(\boldsymbol{x}, t_0)\rangle_{A_{cat}}A_{cat}$; the rate of photon absorption, calculated as $\langle e^a(\boldsymbol{x})\rangle_{V_R}V_R$ and $\langle e^{a,s}(\boldsymbol{x})\rangle_{A_{cat}}A_{cat}$; and the values of the photonic and the quantum efficiency, calculated with Eqs. (2), (3), (5) and (6), are presented in Table 5. It is interesting to note that the mass of TiO_2 in the three reactors, under the selected conditions, is comparable: 27.0 mg in the SR, 21.2 mg in the FFR, and 36.5 mg in the FBR.

As observed in Table 5, the photon absorption rates calculated in the SR and in the FFR were similar. However, the value of η_{Rxn} obtained in the SR was more than twice the value of the FFR. This situation clearly demonstrates that the photons absorbed in the SR are more efficiently employed to degrade CA. The lower interfacial area available for photocatalytic reactions in the FFR could be the reason for the reduction of the efficiency in this reactor.

Considering both reactors with immobilized catalyst, similar reaction rates and photonic efficiencies were obtained. Nevertheless, the value of the photon absorption rate in the FFR was almost twice the value obtained in the FBR. The higher thickness of the TiO_2 film and the more direct illumination in the FFR enhance the absorption of photons and therefore increase the value of the absorbed energy in the reactor. But the FBR offers a higher catalytic area (467.7 cm^2 vs 19.6 cm^2) and a fairly uniform distribution of radiation in the reaction space. As a consequence, the quantum efficiency of the FBR is almost 1.5 times higher than that corresponding to the FFR. This result means that, although the absorbed energy in the FBR is lower than in the FFR, it is more efficiently employed for the photocatalytic reaction.

If we consider the SR and the FBR, the reaction rate obtained in the former reactor triplicates the rate obtained in the second one but, because the absorbed energy in the SR is twice the value of the FBR, the quantum efficiency is only 1.5 times higher. This result suggests that, if we can improve the absorption of photons in the

FBR, we could obtain reaction rates similar to the SR. It is well known that the porosity, the total surface area and the light absorption coefficient of the catalyst are factors that influence the photocatalytic efficiency of a immobilized system. However, the thickness of the films plays a dominant role in the performance of these reactors [3]. Several research studies have shown that the reaction rate increases when increasing the thickness of the films up to an optimum value [8,33,34]. Particularly, in both immobilized systems evaluated in this work, the reaction rate was accelerated when increasing the number of TiO_2 coatings. Therefore, one possible strategy to increase the reaction rate in the FBR is to obtain thicker TiO_2 films over the glass rings, and thus increase the absorption of radiation. This strategy would permit the use of the advantages of the FBR with respect to SR ones and, simultaneously, the achievement of comparable quantum efficiencies.

5. Conclusions

In this work, the performance of three reactor configurations for the photocatalytic degradation of CA is rigorously analyzed. Experimental conditions of maximum reaction rate in each reactor were selected for the comparison.

The lower interfacial area available for photocatalytic reactions in immobilized systems results in a reduction of the efficiency of these reactors in contrast with the suspended system, making the SR the most efficient configuration. Nevertheless, a satisfactory value of the quantum efficiency was obtained in the FBR. Considering all the benefits of the immobilization of the catalyst, the FBR represents a very convenient configuration for photocatalytic reactors.

It is important to remark that an analysis involving only the reaction rates or photonic efficiencies cannot be considered exhaustive to compare different reactor configurations. The analysis of the absorbed radiation is essential to understand the phenomena occurring in photocatalytic reactors and to make improvements in the reactors design.

Acknowledgements

The authors are grateful to Universidad Nacional del Litoral (UNL, CAI+D 2011 501 201101 00335 LI), Consejo Nacional de Investigaciones Científicas y Técnicas (CONICET, PIP 2012 112 201101 00163), and Agencia Nacional de Promoción Científica y Tecnológica (ANPCyT, PICT 2014-1020) for financial support. We also thank Antonio C. Negro for his valuable help during the experimental work.

References

[1] D. Chen, F. Li, A.K. Ray, External and internal mass transfer effect on photocatalytic degradation, Catal. Today 66 (2001) 475–485.
[2] M.F.J. Dijkstra, A. Michorius, H. Buwalda, H.J. Panneman, J.G.M. Winkelman, A. A.C.M. Beenackers, Comparison of the efficiency of immobilized and suspended systems in photocatalytic degradation, Catal. Today 66 (2001) 487–494.
[3] M. Vezzoli, T. Farrell, A. Baker, S. Psaltis, W.N. Martens, J.M. Bell, Optimal catalyst thickness in titanium dioxide fixed film reactors: mathematical modeling and experimental validation, Chem. Eng. J. 234 (2013) 57–65.
[4] N. Vela, J. Fenoll, I. Garrido, G. Navarro, M. Gambín, S. Navarro, Photocatalytic mitigation of triazinone herbicide residues using titanium dioxide in slurry photoreactor, Catal. Today 252 (2015) 70–77.
[5] L. Chen, C. Zhao, D.D. Dionysiou, K.E. O'Shea, TiO_2 photocatalytic degradation and detoxification of cylindrospermopsin, J. Photoch. Photobio. A 307–308 (2015) 115–122.
[6] K. Sivagami, B. Vikraman, R. Ravi Krishna, T. Swaminathan, Chlorpyrifos and Endosulfan degradation studies in an annular slurry photo reactor, Ecotox. Environ. Safe. 134 (2016) 327–331.
[7] C. Berberidou, V. Kitsiou, E. Kazala, D.A. Lambropoulou, A. Kouras, C.I. Kosma, T.A. Albanis, I. Poulios, Study of the decomposition and detoxification of the herbicide bentazon by heterogeneous photocatalysis: kinetics, intermediates and transformation pathways, Appl. Catal. B-Environ. 200 (2017) 150–163.
[8] D. Chen, F. Li, A.K. Ray, Effect of mass transfer and catalyst layer thickness on photocatalytic reaction, AIChE J. 46 (2000) 1034–1045.
[9] G. Camera-Roda, F. Santarelli, Optimization of the thickness of a photocatalytic film on the basis of the effectiveness factor, Catal. Today 129 (2007) 161–168.
[10] M. Vezzoli, T. Farrell, A. Baker, S. Psaltis, W.N. Martens, J.M. Bell, Optimal catalyst thickness in titanium dioxide fixed film reactors: mathematical modeling and experimental validation, Chem. Eng. J. 234 (2013) 57–65.
[11] H. de Lasa, B. Serrano, J. Moreira, P. Valades-Pelayo, Efficiency factors in photocatalytic reactors: quantum yield and photochemical thermodynamic efficiency factor, Chem. Eng. Technol. 39 (2016) 51–65.
[12] M. Motegh, J. Cen, P.W. Appel, J.R. van Ommen, M. Kreutzer, Photocatalytic-reactor efficiencies and simplified expressions to assess their relevance in kinetic experiments, Chem. Eng. J. 207–208 (2012) 607–615.
[13] A. Manassero, M.L. Satuf, O.M. Alfano, Evaluation of UV and visible light activity of TiO_2 catalysts for water remediation, Chem. Eng. J. 225 (2013) 378–386.
[14] I.J. Ochuma, O.O. Osibo, R.P. Fishwick, S. Pollington, A. Wagland, J. Wood, J.M. Winterbottom, Three-phase photocatalysis using suspended titania and titania supported on a reticulated foam monolith for water purification, Catal. Today 128 (2007) 100–107.
[15] D. Li, K. Xiong, W. Li, Z. Yang, C. Liu, X. Feng, X. Lu, Comparative study in liquid-phase heterogeneous photocatalysis: model for photoreactor scale-up, Ind. Eng. Chem. Res. 49 (2010) 8397–8405.
[16] M.E. Leblebici, G.D. Stefanidis, T.V. Gerven, Comparison of photocatalytic space-time yields of 12 reactor designs for wastewater treatment, Chem. Eng. Process. 97 (2015) 106–111.
[17] M.L. Satuf, R.J. Brandi, A.E. Cassano, O.M. Alfano, Quantum efficiencies of 4-chlorophenol photocatalytic degradation and mineralization in a well-mixed slurry reactor, Ind. Eng. Chem. Res. 46 (2007) 43–51.
[18] R. Van Grieken, J. Marugán, C. Sordo, C. Pablos, Comparison of the photocatalytic disinfection of E. coli suspensions in slurry, wall and fixed bed reactors, Catal. Today 144 (2009) 48–54.
[19] A. Dordio, A. Estêvão Candeias, A. Pinto, C. Teixeira da Costa, A. Palace Carvalho, Preliminary media screening for application in the removal of clofibric acid, carbamazepine and ibuprofen by SSF-constructed wetlands, Ecol. Eng. 35 (2009) 290–302.
[20] N.B. Jackson, C.M. Wang, Z. Luo, J. Schwitzgebel, J.G. Ekerdt, J.R. Brock, A. Heller, Attachment of TiO_2 powders to hollow glass microbeads, Activity of the TiO_2-coated beads in the photoassisted oxidation of ethanol to acetaldehyde, J. Electrochem. Soc. 138 (1991) 3660–3664.
[21] S.M. Zacarías, M.L. Satuf, M.C. Vaccari, O.M. Alfano, Efficiency evaluation of different TiO_2 coatings on the photocatalytic inactivation of airborne bacterial spores, Ind. Eng. Chem. Res. 51 (2012) 13599–13608.
[22] G.V. Morales, E.L. Sham, R. Cornejo, E.M. Farfan Torres, Kinetic studies of the photocatalytic degradation of tartrazine, Lat. Am. Appl. Res. 42 (2012) 45–49.
[23] C. Minero, F. Catozzo, E. Pelizzetti, Role of adsorption in photocatalyzed reactions of organic molecules in aqueous titania suspensions, Langmuir 8 (1992) 481–486.
[24] E. Pelizzetti, C. Minero, Electrochim. Acta 38 (1993) 47.
[25] A. Manassero, S.M. Zacarías, M.L. Satuf, O.M. Alfano, Intrinsic kinetics of clofibric acid photocatalytic degradation in a fixed-film reactor, Chem. Eng. J. 283 (2016) 1384–1391.
[26] G. Spadoni, E. Bandini, F. Santarelli, Scattering effects in photosensitized reactions, Chem. Eng. Sci. 33 (1977) 517–524.
[27] T. Yokota, S. Cesur, H. Suzuki, H. Baba, Y. Takahata, Anisotropic scattering model for the estimation of light absorption rates in photoreactor with heterogeneous medium, J. Chem. Eng. Jpn. 32 (1999) 314–321.
[28] G.E. Imoberdorf, G. Vella, A. Sclafani, L. Rizzuti, O.M. Alfano, A.E. Cassano, Radiation model of a TiO_2-coated, quartz wool, packed-bed photocatalytic reactor, AIChE J. 56 (2010) 1030–1044.
[29] R. Siegel, J. Howell, Thermal Radiation Heat Transfer, fourth ed., Taylor and Francis, New York, 2002.
[30] J. Moreira, B. Serrano, A. Ortíz, H. de Lasa, Evaluation of photon absorption in an aqueous TiO_2 slurry reactor using Monte Carlo simulations and macroscopic balance, Ind. Eng. Chem. Res. 49 (2010) 10524–10534.
[31] M. Zekri, C. Colbeau-Justin, A mathematical model to describe the photocatalytic reality: what is the probability that a photon does its job?, Chem Eng. J. 225 (2013) 547–557.
[32] G. Vella, G.E. Imoberdorf, A. Sclafani, A.E. Cassano, O.M. Alfano, L. Rizzuti, Modeling of a TiO_2-coated quartz wool packed bed photocatalytic reactor, Appl. Catal. B-Environ. 96 (2010) 399–407.
[33] S.M. Ould-Mame, O. Zahraa, M. Bouchy, Photocatalytic degradation of salicylic acid on fixed TiO_2 - kinetic studies, Int. J. Photoenergy 2 (2000) 59–66.
[34] N. Padoin, C. Soares, An explicit correlation for optimal TiO_2 film thickness in immobilized photocatalytic reaction systems, Chem. Eng. J. 310 (2017) 381–388.